PSFC/RR-18-3

A wide frequency heterodyne detection method using the Pockels effect

A. Marinoni, C.P. Moeller*, M. Porkolab, J.C. Rost,
E.M. Davis and E.M. Edlund

May 2018

Plasma Science and Fusion Center
Massachusetts Institute of Technology
Cambridge, MA 02139 USA

*General Atomics
P.O. Box 85608
San Diego, CA 92186-5608, USA

This work was supported by the U.S. Department of Energy under DE-SC0016154.

1 Basic theoretical principles of electro-optic modulators

Electro-optic modulators rely on birefringence, which is the optical property of a material having a refractive index that depends on the polarization and propagation direction of light; such anisotropy may be caused by mechanical stresses, electric fields or be intrinsic to the material itself due to its crystalline structure as in the case of calcite.

The impermeability of a general material, η, is defined as

$$\eta \equiv \frac{\epsilon_0}{\epsilon} = \frac{1}{n^2} \tag{1}$$

which makes its variation with the index of refraction, n, equal to

$$\delta\eta = \frac{d\eta}{dn}\delta n = -\frac{2}{n_0^3}\delta n. \tag{2}$$

The index of refraction is generally a complicated function of a number of parameters; however, it is usual practice to consider the electric field, E, and mechanical stresses, σ, to dominate the response. Taking advantage of the fact the variation of the index of refraction is usually very small, the functional dependence of the permeability on electric field and mechanical stress can be expanded in a MacLaurin series as

$$\eta_{ij}(E,\sigma) = \eta_{ij}(0,0) + r_{ijk}E_k + s_{ijkl}E_kE_l + p_{ijkl}\sigma_k\sigma_l \tag{3}$$

with

$$\begin{aligned} r_{ijk} &= \left.\frac{\partial\eta_{ij}}{\partial E_k}\right|_{E=0} \\ s_{ijkl} &= \left.\frac{\partial^2\eta_{ij}}{\partial E_k\partial E_l}\right|_{E=0} \\ p_{ijkl} &= \left.\frac{\partial^2\eta_{ij}}{\partial \sigma_k\partial \sigma_l}\right|_{\sigma=0} \end{aligned} \tag{4}$$

where a sum over repeated indices is assumed. The tensors r and s, which model the response to the applied electric field, are, respectively, the Pockel and the Kerr coefficients; the tensor p models the response to the mechanical stress σ, known as the elasto-optic effect. When the applied electric field and stress tensor are oscillatory in time at sufficient large frequency, as in the case of a modulator considered in this report, p is usually negligible and will not be considered in the following.

By using transpose symmetry and the Shwartz theorem on the order of partial derivatives we can write

$$r_{ijk} = r_{jik} \qquad s_{ijkl} = s_{ijlk} \qquad s_{ijkl} = s_{jikl} \tag{5}$$

leading to a simplification of the representation of the elements; for example,

the tensor r reduces to the following 6 elements

$$\begin{aligned} r_{1k} &= r_{11k} \\ r_{2k} &= r_{22k} \\ r_{3k} &= r_{33k} \\ r_{4k} &= r_{23k} = r_{32k} \\ r_{5k} &= r_{13k} = r_{31k} \\ r_{6k} &= r_{12k} = r_{21k}; \end{aligned}$$

similar relations hold for the s and the η tensors.

For any cartesian coordinate system the equation of the indicatrix has the general form

$$\frac{1}{n_1^2}x^2 + \frac{1}{n_2^2}y^2 + \frac{1}{n_3^2}z^2 + 2\frac{1}{n_4^2}yz + 2\frac{1}{n_5^2}xz + 2\frac{1}{n_6^2}xy = 1. \tag{6}$$

Let us now consider a generic electric field

$$\vec{E} = E_x\hat{x} + E_y\hat{y} + E_z\hat{z} \tag{7}$$

applied to the crystal; eq.3 can be used to calculate the modified indicatrix as follows

$$\begin{aligned} &\left(\frac{1}{n_1^2} + \delta\frac{1}{n_1^2}\right)x^2 + \left(\frac{1}{n_2^2} + \delta\frac{1}{n_2^2}\right)y^2 + \left(\frac{1}{n_3^2} + \delta\frac{1}{n_3^2}\right)z^2 + \\ &2\left(\frac{1}{n_4^2} + \delta\frac{1}{n_4^2}\right)yz + 2\left(\frac{1}{n_5^2} + \delta\frac{1}{n_5^2}\right)xz + 2\left(\frac{1}{n^2} + \delta\frac{1}{n_6^2}\right)xy = 1 \end{aligned} \tag{8}$$

where

$$\delta\frac{1}{n_i^2} = r_{ij}E_j + s_{ijk}E_jE_k \tag{9}$$

Let us now focus on birifringent crystals having favourable properties with light at 10.6 μm, such as CdTe or GaAs. Such crystals belong to the symmetry group $\bar{4}3m$, for which symmetry considerations make the two electro-optic tensors read [1]:

$$r = \begin{bmatrix} 0 & 0 & 0 \\ 0 & 0 & 0 \\ 0 & 0 & 0 \\ r_{41} & 0 & 0 \\ 0 & r_{52} & 0 \\ 0 & 0 & r_{63} \end{bmatrix}$$

$$s = \begin{bmatrix} s_{11} & s_{12} & s_{12} & 0 & 0 & 0 \\ s_{12} & s_{11} & s_{12} & 0 & 0 & 0 \\ s_{12} & s_{12} & s_{11} & 0 & 0 & 0 \\ 0 & 0 & 0 & s_{44} & 0 & 0 \\ 0 & 0 & 0 & 0 & s_{55} & 0 \\ 0 & 0 & 0 & 0 & 0 & s_{66} \end{bmatrix}$$

with $r_{41} = r_{52} = r_{63} = r_{41}$ and $s_{44} = s_{55} = s_{66} = s_{44}$[2].
While all crystals show the Kerr effect, not all of them show the Pockel effect.

If a crystal shows the Pockel's effect, this generally dominates over the Kerr effect.

Let us now consider a crystal cut along its coordinate axis, i.e. [100],[010],[001], and that the applied field is directed along one of these directions; other configurations can be studied in a similar way but the numerical coefficients will obviously be different. In the case the applied electric field is along the x direction, and the Kerr coefficients are neglected, the modified indicatrix reduces to

$$\frac{x^2+y^2+z^2}{n_0^2}+2r_{41}E_x yz=1 \tag{10}$$

where the refractive index is not separated into ordinary and extraordinary components as the crystal is isotropic. Equation 10 can be written without cross products in a new principal system as

$$\frac{x'^2}{n_{x'}^2}+\frac{y'^2}{n_{y'}^2}+\frac{z'^2}{n_{z'}^2}=1 \tag{11}$$

so that $x'=x$; it is convenient to eliminate the cross product by applying a rotation around the $\hat{x}$ axis

$$\begin{aligned} y &= y'\cos(\theta)-z'\sin(\theta) \\ z &= y'\sin(\theta)+z'\cos(\theta) \end{aligned} \tag{12}$$

which transform the indicatrix equation into

$$\begin{aligned} &\frac{x'^2}{n_0^2}+\frac{[y'\cos(\theta)-z'\sin(\theta)]^2}{n_0^2}+\frac{[y'\sin(\theta)+z'\cos(\theta)]'^2}{n_0^2}+ \\ &2r_{41}E_x[y'\cos(\theta)-z'\sin(\theta)][(y'\sin(\theta)+z'\cos(\theta)]=1. \end{aligned} \tag{13}$$

The cross-term $y'-z'$ vanishes identically with a rotation angle $\theta=\pi/4$, for which the indicatrix becomes

$$\frac{x'^2}{n_0^2}+\left(\frac{1}{n_0^2}+r_{41}E_x\right)y'^2+\left(\frac{1}{n_0^2}-r_{41}E_x\right)z'^2=1; \tag{14}$$

therefore, in the new principal system, the refraction index is equal to

$$\begin{aligned} n_{x'} &= n_0 \\ n_{y'} &\simeq n_0\left(1-\frac{1}{2}n_0^2 r_{41}E_x\right) \\ n_{z'} &\simeq n_0\left(1+\frac{1}{2}n_0^2 r_{41}E_x\right). \end{aligned} \tag{15}$$

Let us now consider an amplitude modulator composed of two linear polarizers rotated by 90 degrees with respect to each other, and a crystal in between them subject to an electric field along the $\hat{x}$ direction (see Figure 1).

The electro-magnetic wave enters the crystal with the following polarization

$$\vec{E}=E_0\frac{\sqrt{2}}{2}(\hat{x}+\hat{y})e^{-\imath\omega t} \tag{16}$$

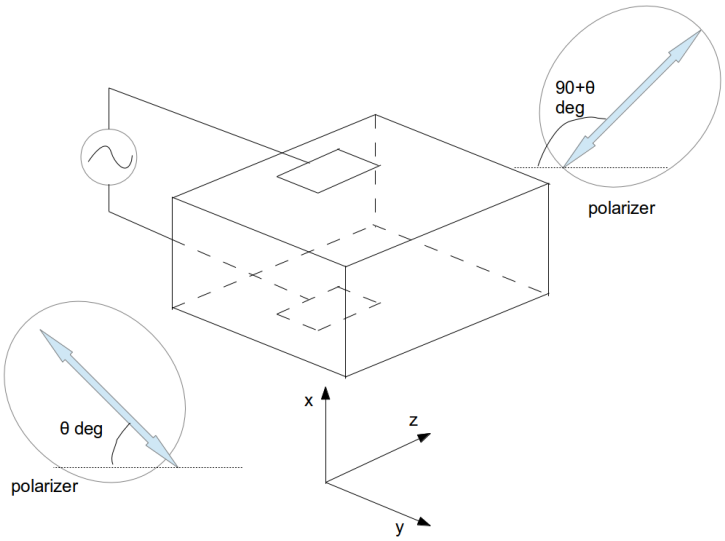

Figure 1: Sketch of the amplitude modulator

which corresponds to $\theta = \pi/4$ in Fig.1. If the crystal has dimensions (d, d, L), after the wave has propagated through its length L the electric field reads

$$\vec{E} = E_0 \frac{\sqrt{2}}{2} \left[\hat{x} + \hat{y} \cdot exp\left(-\imath \frac{1}{2} k_0 L n_0^3 r_{41} E_x \right) \right] e^{\imath n_0 k_0 L} e^{-\imath \omega t}, \tag{17}$$

which shows that the applied electric field induces a phase difference, 2δ, between the x and y components equal to

$$2\delta = \frac{1}{2} k_0 L n_0^3 r_{41} E_x. \tag{18}$$

The wave electric field at the exit face of the crystal, discarding isotropic phase factors, can therefore be written as

$$\vec{E} = E_0 \frac{\sqrt{2}}{2} \left(\hat{x} e^{-\imath\delta} + \hat{y} e^{+\imath\delta} \right) \tag{19}$$

which, after projection onto the exit polarizer oriented along $\hat{n} = (\hat{x}, \hat{y})$, becomes

$$\vec{E} = \imath E_0 \sin(\delta) \vec{n} \tag{20}$$

which translates into a beam intensity equal to

$$I = I_0 \sin(\delta)^2. \tag{21}$$

In order to achieve the desired modulation, one possibility would to bias the crystal at $V_{\pi/2}$, i.e. $2\delta = \pi/2$ which gives I/I_0=0.5, and modulate as close as possible to $\delta = \pm\pi/4$; the required voltage would then be equal to

$$2\frac{\pi}{4} = \frac{1}{2} k_0 L n_0^3 r_{41} \frac{V_{\pi/2}}{d} \Longrightarrow V_{\pi/2} = \frac{\lambda_0 d}{2 n_0^3 r_{41} L}. \tag{22}$$

Alternatively, the intensity modulation can be made linear in $\sin(\delta)$ by applying a quarter wave plate between the two polarizers, so that

$$I = I_0 \sin(\delta + \pi/4)^2 = \frac{1 + \sin 2\delta}{2} \tag{23}$$

without any DC biasing voltage. For an on-off modulation 2δ needs to be equal to $\pi/2$, which gives

$$\frac{\pi}{2} = \frac{1}{2} k_0 L n_0^3 r_{41} \frac{V_{on-off}}{d} \tag{24}$$

or

$$V_{on-off} = \frac{\lambda_0 d}{2 n_0^3 r_{41} L} \tag{25}$$

Since the modulator considered in this report will have to operate with light at 10.6 μm wavelength, the choice of birefringent crystals is restricted to those which do not significantly attenuate light at such wavelength. Suitable materials are CdTe, ZnSe, GaAs and ZnTe which belong to the crystallograhic group $\bar{4}3m$; numerical values of electro-optic coefficients and refraction indices of such crystals are taken from [4] and reported in Tab.1.

Material Unit	r_{41} [10^{-12} m/V]	n_0 []	$r_{41} n_0^3$ [10^{-12} m/V]	ρ [10^8 Ωcm]
CdTe	6.8	2.60	120	1
GaAs	1.51	3.30	54	10
ZnSe	2.2	2.39	30	10^4
ZnTe	3.9	2.7	78	n.a.

Table 1: Electro-optic coefficient and refraction index measured with 10.6 μm wavelength light for materials belonging to the symmetry group 43m. The last column indicates the undoped electrical reistivity.

For CdTe of dimensions [5,5,50] mm (quote from II-VI 261092) at $\lambda_0 = 10.64$ μm, $n_0^3 r_{41} = 1.2 \cdot 10^{-10}$ m/V, so that the required voltage is equal to 4433 V. Note that this value corresponds to a wave amplitude; its the peak-to-peak and rms values would be twice and half that value, respectively.

Let us now consider a more arbitrary cut, for which the light does not necessarily propagate along one of the crystallographic axes. For a $\bar{4}3$m crystal, for which $n_x = n_y = n_z = n_0$, the indicatrix reads

$$\frac{x^2 + y^2 + z^2}{n_0^2} + 2 r_{41} (E_x yz + E_y xz + E_z xy) = 1; \tag{26}$$

the index of refraction in the principal coordinate system are found by diagonalizing the matrix

$$\begin{bmatrix} \frac{1}{n_0^2} & r_{41} E_z & r_{41} E_y \\ r_{41} E_z & \frac{1}{n_0^2} & r_{41} E_x \\ r_{41} E_y & r_{41} E_x & \frac{1}{n_0^2} \end{bmatrix}$$

By cutting and orienting the crystal in the way sketched in figure 2, which corresponds to having:

- the electrode surfaces along $(1\bar{1}0)$

- the side surfaces along (001)
- the optical surfaces along (110)

we obtain that $\pm E_x = \mp E_y = \pm E_0/\sqrt{2}$ and E_z=0, which makes the eigenvalues equal to $(n_0^{-2} + r_{41}E_0, n_0^{-2} - r_{41}E_0, n_0^{-2})$. By assuming again that the perturbation to the refraction index is much smaller than one, by Taylor expanding to first order we obtains

$$\begin{aligned} n_{x'} &= \frac{n_0}{\sqrt{n_0^2 + r_{41}E_0}} \simeq n_0 - \frac{n_0^3 r_{41} E_0}{2} \\ n_{y'} &= \frac{n_0}{\sqrt{n_0^2 - r_{41}E_0}} \simeq n_0 + \frac{n_0^3 r_{41} E_0}{2} \\ n_{z'} &= n_0 \end{aligned} \tag{27}$$

and the directions of the normal modes are along

$$\begin{aligned} \hat{x}' &= \frac{\hat{x} - \hat{y} + \sqrt{2}\hat{z}}{2} \\ \hat{y}' &= \frac{-\hat{x} + \hat{y} + \sqrt{2}\hat{z}}{2} \\ \hat{z}' &= \frac{\hat{x} + \hat{y}}{\sqrt{2}}. \end{aligned} \tag{28}$$

When the probing electric field is polarized along the vertical direction in figure 2, Eq.17 becomes

$$\vec{E} = E_0 \frac{\sqrt{2}}{2} \left[\hat{x} exp\left(-\imath \frac{1}{2} k_0 L n_0^3 r_{41} E_0 \right) - \hat{y} exp\left(\imath \frac{1}{2} k_0 L n_0^3 r_{41} E_0 \right) \right] e^{\imath n_0 k_0 L} e^{-\imath \omega t} \tag{29}$$

and the phase difference between the $\hat{x}$ and $\hat{y}$ components becomes equal to

$$2\delta = k_0 n_0^3 L r_{41} E_0 \tag{30}$$

which halves the quarter-wave (on-off) voltage, bringing it down to about 1760 V. Table 2 reports all on-off voltages required for the crystals listed in Table 1.

Material	V_{on-off} [V]
CdTe	2217
GaAs	4926
ZnSe	8867
ZnTe	3410

Table 2: On-off voltages for materials in Table 1 with the electric field in the 110 direction and light polarized along the 001 plane.

Another feasible crystal cut would be such that the biasing electric field is in the 111 direction, with the maximum phase shift equal to

$$2\delta = \frac{\sqrt{3}\pi L}{\lambda d} n_0^3 r_{41} V \tag{31}$$

which is a factor $2/\sqrt{3}$ less than that given by Eq.30.

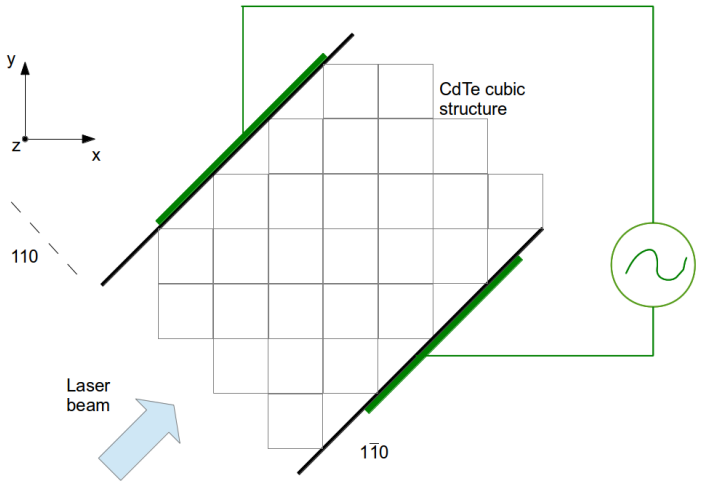

Figure 2: Top view of the crystal in the crystallographic reference frame. The crystal will be cut along the planes $(110, 1\bar{1}0, 001)$, 001 being the horizontal plane. The laser beam would be polarized along the 001 direction.

2 Transit time limitation

If the length of the crystal and the modulation frequency are such that the transit time of the light was equal to the inverse of the modulation frequency, then there would not be any net power modulation as the phase shifts experienced at the beginning of the crystal would cancel those at the end.
The transit time of light in a crystal of length L and refraction index n is

$$\tau = \frac{Ln}{c}, \tag{32}$$

for this to be negligible compared to the modulation frequency f_m, the latter should be such that $f_m\tau \ll 1$. As the modulation frequency increases and becomes comparable to the transit time, the modulator does not respond adiabatically anymore to the time varying index of refraction. Let us write the phase retardation as [3]

$$2\delta = aLE \tag{33}$$

where L is the length of the crystal, E the intensity of the electric field, and a a factor that takes into account the geometry of the system. When the transit timeaffects the overall modulation depth, the elementary phase retardation along the crystal is given by

$$d(2\delta) = aE(x)dx \tag{34}$$

where x is the coordinate along the direction of propagation and assumes values between 0 and L. The system is such that light is at $x = L$ at time t and at $x = 0$ at time $t - \tau$, which makes

$$x = \frac{c}{n}(t_x - t + \tau). \tag{35}$$

Assuming $E = E_0 \cos(2\pi f_m t + \phi)$, the total phase retardation is therefore equal to

$$\begin{aligned} 2\delta &= \int_0^L dx E(x) = E_0 \frac{c}{n} \int_{t-\tau}^{t} dt \cos(2\pi f_m t + \phi) \\ &= E_0 \frac{c}{n 2\pi f_m} \left[\cos\left(2\pi \left(t - \frac{\tau}{2} + \phi\right)\right) \sin\left(\frac{2\pi\tau}{2}\right)\right] \end{aligned} \tag{36}$$

Comparing equations 33 and 36 we see that the transit time will reduce the efficacy of the modulator by a factor ρ

$$\rho = \frac{\sin\left(\frac{2\pi f_m \tau}{2}\right)}{\frac{2\pi f_m \tau}{2}}. \tag{37}$$

Typical modulation frequencies of interest for this report are ten of MHz for detection of Ion Cyclotron Emission, one half GHz for detection of the Helicon way as it is being designed for the DIII-D tokamak, and a few GHz for detection of the Lower Hybrid wave. Considering a CdTe crystal of length $L = 50$ mm, the reduction of the efficiency of the modulator is equal to 99.9%, 92.4% and 19.8%, respectively, for the three frequencies above; second order differences are found for the other crystals considered in this report. A traveling wave modulator is therefore required only for frequencies that reach or exceed 1 GHz, as required by detection of Lower Hybrid waves.

3 Higher order harmonics

The electro-optic cell produces an intensity modulation which, as seen in eq. 23, is a sinusoidal function of the phase shift, which is linear in the applied voltage. In the case of a sinusoidally varying voltage, the intensity modulation will feature higher order harmonics. Indeed, the Jacobi-Anger equation

$$e^{\imath z \cos\theta} = \sum_{n=-\infty}^{\infty} \imath^n J_n(z) e^{\imath n \theta} \tag{38}$$

can be used together with Euler's formula to compute the harmonic expansion of eq. 23

$$\sin[z\cos(\theta)] \equiv \frac{e^{\imath z\cos(\theta)} - e^{-\imath z\cos(\theta)}}{2\imath} = \sum_{n=\infty}^{\infty} \imath^{2n} J_{2n+1}(z) e^{\imath(2n+1)\theta} \tag{39}$$

which shows that the strength of the n-th harmonic is the n-th order Bessel function of the first kind, and that even harmonics do not contribute to the signal. The argument of the Bessel function, z, is the maximum phase shift between the ordinary and the extraordinary components of the laser beam which, for realistic parameters, is between zero, which corresponds to no applied voltage, and $\pi/2$, which corresponds to the on-off modulation depth. A quantitative representation of the relative strengths of various harmonics compared to the fundamental as a function of the modulation depth is given in fig.3. In particular, by imposing that the amplitude of the first spurious component, i.e. that at

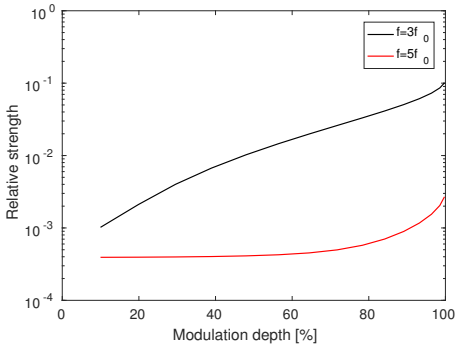

Figure 3: Amplitude of higher components, relative to that of the fundamental frequency, in the intensity of the modulated beam as a function of the modulation depth.

three times the fundamental frequency, in the intensity of the modulated beam is at most one-hundredth of that at the fundamental frequency, we obtain that the modulation depth cannot exceed 50%, or one-third the quarter-wave voltage. Higher components are well below one-thousandth for almost all possible values of the modulation depth, and are therefore not expected to significantly bias the heterodyne detection scheme.

While the presence of third and higher order harmonics does not represent an appreciable issue for the detection of the Helicon or Lower Hybrid waves due their large and fixed frequency, it does trouble the heterodyne detection of broadband fluctuations such as Ion Cyclotron Emission (*ICE*). Indeed, let us assume that the Pockel cell is set to modulate at a frequency of 8 MHz; any plasma wave oscillating around 24 MHz within the detector bandwidth will be detected by the optical heterodyne scheme, therefore biasing the analysis. In case a 100% modulation depth was required, e.g. for S/N considerations, one remedy to the higher order harmonics would be to modulate the voltage with a triangular waveform, so that an almost pure sinusoidal intensity modulation would be obtained. A calculation similar to the one that generated fig.3 indicates that the spectral contamination at all orders is less than one-thousands at modulation depths larger than 98%. However, such scheme would produce a spectral contamination higher than one-tenth at $f = 3f_0$ for a modulation depth less than 75%, or half the quarter-wave voltage.

4 Dielectric losses

In a purely capacitive component such as a Pockels cell, dielectric losses are the primary cause of power dissipation in the system and, therefore, determine the power to be provided by the RF driver as well as that to be removed by the cooling system.

In order to determine the dielectric losses it is useful to very briefly review the basic theory of the complex dielectric constant in materials. The simplest model for the non relativistic dynamics of a bound electron under an external

electric field E, can be expressed as

$$m\ddot{\mathbf{r}} = e\mathbf{E} - k\mathbf{r} - m\gamma\dot{r} \tag{40}$$

where m is the electron mass, e its electric charge, k a spring-like force attracting the electron to its nucleus and γ represents a viscous-type force that depends linearly on the velocity of the electron. For the sake of simplicity we assume the external field to be aligned along one of the axis of the reference frame, so that the vector notation can be dropped and k be expressed as a constant. By defining $\omega_0 \equiv \sqrt{k/m}$ we obtain

$$\ddot{r} + \gamma\dot{r} + \omega_0^2 r = \frac{e}{m}E, \tag{41}$$

for which the following limits apply:

1. Dielectric: $\omega_0 \neq 0$, $\gamma \neq 0$
2. Conductor: $\omega_0 = 0$, $\gamma \neq 0$
3. Collisionless plasma: $\omega_0 = 0$, $\gamma = 0$.

The form of eq. 41 implies that a sinusoidal electric field of the form $E(t) = E_0 e^{\imath\omega t}$ would produce a similar time dependence for the displacement of the electron, whose solution at any frequency ω is given by

$$r = \frac{e}{m}\frac{E}{\omega_0^2 - \omega^2 + \imath\omega\gamma}; \tag{42}$$

this results in the polarization per unit volume to be equal to

$$P \equiv Np = Ner \equiv \frac{Ne^2}{m}\frac{E}{\omega_0^2 - \omega^2 + \imath\omega\gamma} \equiv \epsilon_0\xi(\omega)E \tag{43}$$

with the displacement field, D, given by

$$D = \epsilon_0 E + P = \epsilon_0(1 + \xi(\omega)E = \epsilon(\omega)E. \tag{44}$$

By defining the plasma frequency, ω_p, as

$$\omega_p^2 = \frac{Ne^2}{\epsilon_0 m} \tag{45}$$

the effective permittivity can be expressed as

$$\epsilon(\omega) = \epsilon_0\left[1 + \frac{\omega_p^2}{\omega_0^2 - \omega^2 + \imath\gamma\omega}\right] = \epsilon'(\omega) - \imath\epsilon''(\omega), \tag{46}$$

the real and the imaginary parts of which are referred to as the refractive and absorbing parts, respectively. When $\omega \simeq \omega_0$ the material goes through a resonance, with the real part of the permittivity decreasing with ω and therefore showing an anomalous dispersion, while the imaginary part of the permittivity shows a lorentzian behavior around ω_0. Usually a material exhibits several frequencies corresponding to a variety of vibrational modes, so that the permittivity can be written as

$$\epsilon(\omega) = \epsilon_0 \left[1 + \sum_{i=1}^{M} \frac{\omega_{p,i}^2}{\omega_i^2 - \omega^2 + \imath\gamma_i\omega} \right]. \tag{47}$$

A formal quantum mechanical treatment [10] leads to

$$\epsilon(\omega) = \epsilon_0 \left[1 + \frac{e^2\epsilon_0}{m} \sum_{i=1, j>i}^{M} \frac{f_{ji}(N_i - N_j)}{\omega_{ji}^2 - \omega^2 + \imath\gamma_i\omega_{ji}} \right]. \tag{48}$$

where $\omega_{ji} \equiv (E_j - E_i)/\hbar$ is the transition frequency between energy levels i and j, N_i is the population of the lower energy level E_i and N_j that of the upper level E_j, and f_{ji} are called oscillator strengths. Lower energy states are generally more populated, causing the material to behave as an absorbing dielectric. However, in case of a population inversions, i.e. $N_i < N_j$, the permittivity changes sign and the material shows a gain in the neighborhood of the resonance.

In general, a given material shows both dielectric and conductive properties at different frequencies, so that a simple model of its permittivity would then be

$$\epsilon(\omega) = \epsilon_0 \left[1 + \frac{\omega_{d,p}^2}{\omega_{d,0}^2 - \omega^2 + \imath\gamma_d\omega} + \frac{\omega_{c,p}^2}{\imath\omega(\imath\omega + \gamma_c)} \right] \equiv \epsilon_d(\omega) + \frac{\sigma_c(\omega)}{\imath\omega} \tag{49}$$

where subscripts d, c stand for dielectric and conductive, respectively; in such case the Ampere's law gives

$$J_{tot} = J + \frac{\partial D}{\partial t} = \sigma_c(\omega)E + \imath\omega\epsilon_d(\omega)E = \imath\omega\epsilon(\omega)E. \tag{50}$$

The relative strength between the conduction and the displacement currents determines whether the material behaves as a conductor or as a dielectric. By separating the total permittivity into its real and its imaginary parts, the total current reads

$$J_{tot} = \imath\omega\epsilon(\omega)E = \imath\omega\epsilon'(\omega)E + \epsilon''(\omega)\omega E \tag{51}$$

and the Joule losses per unit volume can be written as

$$\frac{dP_{loss}}{dV} = \frac{1}{2}\langle JE^* \rangle_T = \frac{1}{2}\epsilon''(\omega)\omega|E|^2 \tag{52}$$

which shows that the losses are a linear function of the frequency.

Let us assume that, at least in the frequency range of interest, $\sigma_c(\omega)$ is real-valued. It follows from eq. 49 that

$$\epsilon''(\omega) = \epsilon_d''(\omega) + \frac{\sigma_c(\omega)}{\omega} \tag{53}$$

and the ohmic losses can be written as

$$\frac{dP_{loss}}{dV} = \frac{1}{2}[\omega\epsilon_d''(\omega) + \sigma_c(\omega)]|E|^2. \tag{54}$$

It is convenient to characterize ohmic losses through a parameter called *loss tangent*, which is defined by

$$\tan\theta \equiv \frac{\epsilon''(\omega)}{\epsilon'(\omega)} = \frac{\sigma_c + \omega\epsilon''_d(\omega)}{\omega\epsilon'_d(\omega)} = \frac{\sigma_c(\omega)}{\omega\epsilon'_d(\omega)} + \frac{\epsilon''_d(\omega)}{\epsilon'_d(\omega)} \equiv \tan(\theta_c) + \tan(\theta_d). \quad (55)$$

Ohmic losses can then be written in terms of the loss tangent parameter as

$$\frac{dP_{loss}}{dV} = \frac{1}{2}\omega\epsilon'_d(\omega)\tan(\theta)|E|^2. \quad (56)$$

According to [11], at frequencies equal to 15.95 and 60 GHz, the loss tangent for CdTe was measured to be $1.1 \cdot 10^{-2}$ and $1.5 \cdot 10^{-2}$, respectively; while the dielectric constant was measured to be equal to 10.31 ± 0.08 and 10.39 ± 0.04 at 1 MHz and 15.95 GHz, respectively. Assuming that such values do not significantly vary over frequency by going to the tens of MHz range, in our CdTe crystal ($5 \times 5 \times 50\ mm^3$ subject to 1 kV oscillating at in the 10-20 MHz frequency range) dielectric losses can be estimated to less than 1 W. Design safety would estimate dielectric losses to a few watts, which is the power that has to be provided by the RF driver and dissipated by the cooling system. Dielectric losses for the Helicon wave are estimated by a simple extrapolation of eq. 56 at the frequency of the Helicon wave, at fixed volume, to about 20 W.

5 Actual Cell

Even though CdTe provides the best performance and is therefore the first choice crystal, only a few companies have the necessary equipment and certification to legally handle it because of its inclusion in national and international toxicology programs. Most of the companies that were contacted work only with ZnSe or GaAs, no company offered ZnTe. An extensive vendor search identified II-VI (USA), Gooch&Housego (UK) and Hyvel (USA) as potential providers of a CdTe crystal along with a prototype housing, but were unable to provide a suitable RF driver; the german company Qubig was identified as a provider of a complete modulator composed of a number of resonant cavities that would drive a GaAs crystal at various frequencies. Official quotes were obtained for the CdTe cell from the three companies above, while subtle technicalities that are beyond the scope of this report prevented QuBig from providing an official quote, even though simulations indicated that a suitable modulation depth would be achieved in the range of tens of MHz.

II-VI inc. was chosen as provide of the cell based their cost competitive quote and on their history of reliability. The quote from Gooch&Housego was rejected because it exceeded the budget available to this project, while that from Hyvel because, besides being more expensive than that from II-VI, raised concerns regarding the cooling system of the cell; indeed, instead of cooling ceramic components in direct contact with the crystal, their design relied on an a chamber filled with nitrogen gas to be used as an intermediate layer between the water pipes and the crystal. While possibly minimizing the risk of creating moisture, such design would have increased maintenance overhead as the quantity of nitrogen gas would have had to be constantly monitored in order to avoid damage to the crystal.

After a few iteration with II-VI regarding the dimensions of the crystal, an official quote for a water cooled Pockels cell was obtained. The size of the crystal was a compromise between cost, which scales with size, clear aperture, which is to be kept as large as possible for alignment issues, and cross-section, which has to be minimized in order to lower the voltage required to drive the cell. It was decided to order a crystal whose dimensions are $5 \cdot 5 \cdot 50$ mm^3, where the longer dimension is along the light propagation. The crystal would be cut along the Miller planes $(110, 1\bar{1}0, 001)$, resulting in the configuration depicted in Fig.4 Based on the design of the RF circuit that was being designed to drive

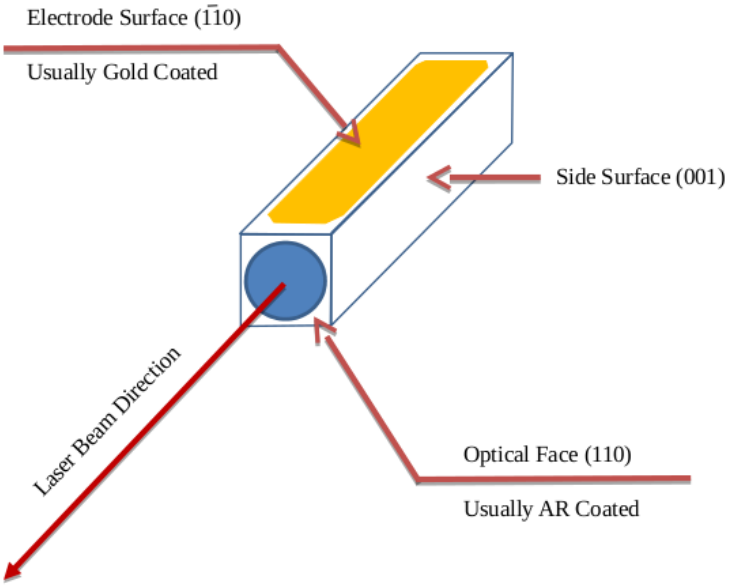

Figure 4: Cartoon representing the CdTe crystal and its Miller indexes compared to the direction of propagation of the laser beam

the cell, it was decided to connect one of the two plates of the capacitor to ground, as opposed to have both terminals floating. An MHV connector was preferred over soldering pins for obvious practical reasons. Based on previous work and literature, II-VI estimated the electrical resistance and capacitance of the cell to about 100 MΩ and 10 pF which, at 25 and 476 MHz frequency, translate into about 630 and 33 Ω impedance, respectively. Every crystal has a breakdown voltage whose value depends on the ambient conditions in which the crystal is, mainly temperature and pressure. For this reason II-VI did not quote a breakdown voltage, even though they stated that the CdTe crystal should be able to withstand 1 kV per millimeter; for the crystal of our choice, this limit would translate into 5 kV. However, safety considerations would impose to lower such limit by 20%, setting the final value to 4 kV. It should be noted that the afore-mentioned breakdown limit was verified only at modulation frequencies of 200 kHz or less. The optical faces of the crystal will be coated for anti-reflection at 10.6 μm wavelength only, the additional cost of depositing a double band AR coating layer to accommodate a visible HeNe was deemed as not necessary.

In view of the large investment in the crystal and the exploratory nature of this work, a relatively inexpensive test crystal, made of ZnSe, was also ordered in an identical housing. The two crystals have similar electrical properties, though the ZnSe is less efficient at modulating the laser, so the ZnSe crystal will be used to verify that the drivers deliver the appropriate high voltage at the design frequency without causing breakdown in the crystal, while the CdTe crystal will be used for physics studies.

The actual CdTe cell as built by II-VI is shown in figure 5. Its capacitance was measured to be equal to 15 pF, its clear aperture is 4 mm and can be operated with a laser beam impinging on the crystal with at 2 degrees; a picture is displayed in fig.5.

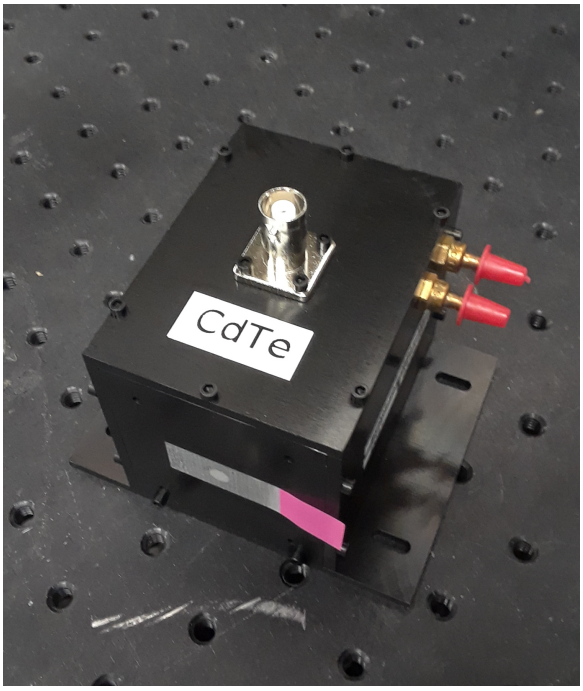

Figure 5: Picture of the actual CdTe cell. The MHV connector can be seen on the top, along with the entry and exit water pipes for active cooling. The crystal is protected with lens tissue.

6 Modulation depth for Helicon

In this section we will review the expected signal to noise ratio in an heterodyne phase contrast diagnostic, and derive the minimum modulation depth necessary for the detection of the helicon wave; no such estimate can be made for *ICE* due to the lack of theoretical prediction regarding the induced density perturbation.

Let us consider a heterodyne detection scheme based on a sinusoidal modulation of the probing laser beam power. The time evolution of the intensity of the laser beam can be written as

$$I(t) = \alpha I_0 + \beta I_0 \cos(\omega_m t) \tag{57}$$

where I_0 is the unmodulated intensity, α is a positive correction factor that accounts for losses in the modulator, β determines the modulation depth, and ω_m is the angular frequency of the modulation. It is understood that $0 \leq \alpha \leq 0.5$, $0 \leq \beta \leq \alpha$ as the intensity cannot be negative. Also, the modulation is assumed to be homogeneous across the probing beam wavefront, so that spatial coordinates can be omitted for simplicity. The non-fluctuating PCI signal will have a DC component as well as a component oscillating at ω_m, while the signal scattered by plasma waves at frequency ω will appear at ω, its natural frequency, and at $\omega \pm \omega_m$. When the modulating frequency is equal to tens, or hundreds, of megahertz, the two sidebands are well spaced apart so that only one sideband can usually be measured.
Let us now compute the S/N ratios of a single sideband heterodyne detection. The voltage responsivity of the detector can be written as

$$V_s(t) = \Re A_e \tilde{I}(t) \tag{58}$$

where A_e is the area of the detector element, $\Re$ the voltage responsivity, and $\tilde{I}$ the fluctuating intensity of the laser beam impinging on the detector. Equation 58 can be expressed as a function of the fluctuating phase of the probing beam as [5]

$$V_s(t) = \Re A_e T(\infty) W \tilde{\phi}(t) \tag{59}$$

where W and T account for the transfer function of the system.
Detector noise can be usually cast into two main form: shot-noise and intrinsic noise, which incorporates the contributions from *1/f, Thermal Johnson and Generation-Recombination* processes. The former is a statistical noise due to the quantum nature of light, while the latter is described by a parameter called *apparent detectivity*, D^*, and is commonly used to characterize detectors. The shot-noise in a photocnductive detector is given by [6]

$$V_{LO}^2 = F_d \Re^2 A_e \Delta f \frac{\hbar \omega_0}{\eta} I_0 \tag{60}$$

where η is the quantum efficiency of the detector, Δf the bandwith and ω_0 the angular frequency of the incident radiation; F_d, a factor that takes into account recombination effects, is equal to two for PC devices and unity for PV devices. The rms value of the intrinsic noise is given by

$$V_{intr}^2 = \frac{\Re^2 A_e \Delta f}{D^{*2}}. \tag{61}$$

The signal to noise ratio can be calculated as

$$S/N = \frac{V_s^2}{V_{LO}^2 + V_{intr}^2} = \frac{A_e}{\Delta f} \frac{\left[T(\infty) W \tilde{\phi}\right]^2}{\frac{1}{D^{*2}} + 2 F_d I_0 \frac{\hbar \omega_0}{\eta}} \tag{62}$$

by computing the transfer function one can replace Eq.62 by

$$S/N = \frac{4 A_e}{\Delta f} \frac{\left[I_0 \tilde{\phi}\right]^2}{\frac{1}{D^{*2}} + 2 F_d I_0 \frac{\hbar \omega_0}{\eta}} \tag{63}$$

within 5% accuracy.

Let us now estimate the change in the S/N ratio when we adopt a heterodyne scheme, modeled by Eq.57, with single sideband detection. The signal drops by a factor $\beta/2$, where the factor of two is due to the single sideband detection and decreases the rms voltage by $\beta^2/4$. The shot noise rms decreases by a factor equal to α, while detector noise is unmodified. Since we forced the conditions $\beta \leq \alpha$ and $\alpha \leq 1/2$, the intensity out of the modulator is less, or at most equal, to the intensity out of the laser. The S/N ratio in the heterodyne scheme normalized to that in an homodyne one is equal to:

$$\frac{(S/N)_{het}}{(S/N)_{hom}} = \begin{cases} \frac{\beta^2}{4}, & \text{if intrinsic noise dominates.} \\ \frac{\beta^2}{4\alpha}, & \text{if shot noise dominates.} \end{cases} \tag{64}$$

these two factors are plotted in Fig.6 and are limited to 1/8 and 1/16, respectively, when $\alpha = \beta = 0.5$, i.e. for a lossless modulator with 100% modulation depth.

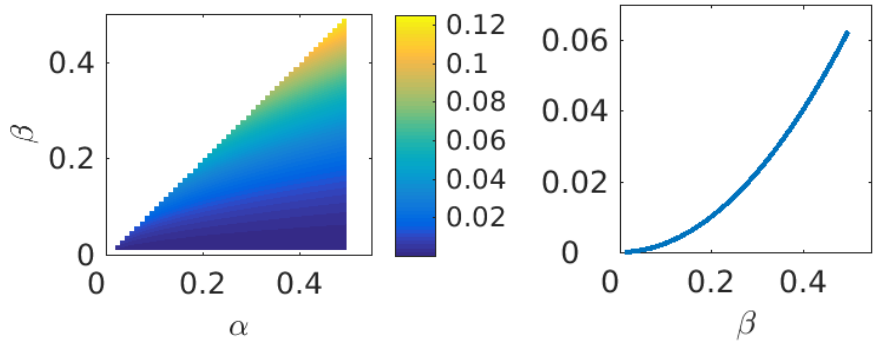

Figure 6: Reduction in S/N ratio from homodyne to heterodyne, single sideband, detection scheme for a shot noise dominated (left) and an intrinsic noise dominated case (right).

Let us now evaluate the requirements to detect the Helicon wave with the PCI as installed on the DIII-D tokamak.
Based on two dimensional full wave AORSA modeling, the Helicon wave is expected to produce a phase perturbation to the probing laser beam of the order of 1–5 $\times$ 10^{15} $\mathrm{m}^{-2}\mathrm{MW}^{-1/2}$ [7] which, considering an antenna able to couple 1 MW to the plasma, translates into a phase perturbation in the interval 0.03–0.15 mrad. Let us take the values in Tab.3 to set the parameters in Eq.63.

Detector	A_e [mm^2]	Δf [kHz]	D^* [$\mathrm{cm} \cdot \mathrm{Hz}^{1/2}/\mathrm{W}$]	η []
PC	0.5	300	$3 \cdot 10^{10}$	0.8
PV	0.16	300	10^9??	0.02

Table 3: DIII-D PCI parameters to be used in Eq.63

The peak intensity of a gaussian beam of total power P, waist w at $1/e$ points in electric field w is equal to $I_0 = 2P/(\pi/w^2)$. By assuming $P = 5$ W, $w_0 = 3.5$ cm and $M = 0.2$, we obtain $I_0 = 6.5$ $\mathrm{W/cm}^2$. The S/N ratios, in case

the helicon wave will be detected a few hundreds of kHz away from its nominal value, assume the following estimated values

$$(S/N)_{hom} = \begin{cases} 10^3\text{–}10^4 & \text{for the PC detector} \\ 10^2\text{–}10^3 & \text{for the PV detector} \end{cases} \tag{65}$$

Let us assume that the heterodyne detection scheme needs to retain a S/N ratio equal to, at least, 10; then, in the worst case of the PC detector, the impact on the S/N ratio due to the heterodyne detection has to be less or equal to 100. By looking at Eqs.23 and 57 we can set $\alpha = 0.5$ and $\beta = \sin(2\delta)/2$. Assuming that the detector will operate in a region somewhere in between the shot noise and the intrinsic noise dominated regimes, we can assume that the reduction in the S/N ratio will be an average of the two limits expressed in Eq.64, i.e. $3\beta^2/8$, which gives $\beta \simeq 0.16$. This, in turns, means that $2\delta \simeq 0.32$ and the required modulated voltage to be applied to the birefrengent crystal is about one-fifth of the on-off voltage, i.e. about 360 V.

7 RF-Circuitry

The development of an RF circuitry for the helicon wave and for the detection of fluctuations in a broadband region at lower frequency, such as *ICE*, generally requires two different approaches. While the circuitry for the helicon wave can be realized with some sort of resonant circuit at a fixed frequency, i.e. that of the wave, *ICE* requires a circuitry able to make the Pockels cell oscillate at various frequencies in a given range or, even better, continuously in a broadband frequency region. Another difference between the two circuitries relies in the dielectric losses; indeed, as derived in the sec. 4, the dielectric losses at the *ICE* frequency range require the RF driver to provide a negligible amount of power, while an RF circuit at the Helicon frequency would have to provide approximately 20W, which is at the limit of low cost, broadband rf amplifiers available in the market for less than 5000 $.

The voltage requirements for electro-optic cells considered in this white paper are around 2 kV peak-peak, or 700 V rms. The equivalent circuit for a Pockels cell can be described as a large resistor, which based on data reported in Tab.1 is estimated in about 20 MΩ, in parallel to a capacitor having a DC capacitance of the order of 15 pF, which represent the capacitance of the crystal along with that of its housing. The extremely large value of such resistor is such that it is dominated by the equivalent resistor modeling the loss tangent which, depending on the frequency, varies between 25 kΩ and 2 MΩ. At RF frequencies, the capacitance of cables cannot be neglected and usually amounts to 100 pF/m for 50Ω impedance cables; lower capacitance values can be obtained at higher impedance. A schematic representation of the equivalent circuit is displayed in fig. 7.

In view of considerations expressed in sec. 3, the design voltage should be approximately 1 kV amplitude without any DC offset, resulting in voltage-current parameters expressed in Tab.4

The large Volt-Ampere-Reactive values reported in 4 are such that some form of resonant circuit is needed to achieve the required voltage. Solutions include a tank circuit and/or a step-up transformer. An alternative approach

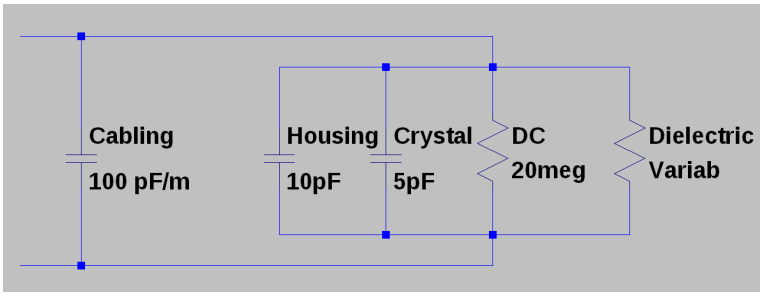

Figure 7: Schematic representation of the equivalent circuit of a Pockels cell, including the capacitance of the crystal, that of the enclosure and of the cables delivering the voltage to the cell, the DC resistance of the crystal and that representing dielectric losses.

Frequency [MHz]	10	20	30	60	476
Impedance cell [Ω]	-$\imath$1061	-$\imath$530	-$\imath$354	-$\imath$177	-$\imath$22
Current cell [A]	-$\imath$0.94	-$\imath$1.88	-$\imath$2.83	-$\imath$5.65	-$\imath$44.86
Power cell [kvar]	0.46	0.92	1.38	2.76	22.27

Table 4: Overview of voltages and currents driven through the circuit by an RF amplifier able to drive 2 kV p-p at any given frequency in the table.

would be to use resonant cavities with high quality factor, Q. In order to avoid harmonic contamination, large Q values are required and, therefore, multiple cavities are needed if an extended frequency bandwidth is to be covered.

Let us now describe three viable solutions for the circuitry at a few tens of MHz. The first solution consists of a series of resonant cavities to be connected, one at a time, to the cell. A feasibility study was made with the german company *Qubig* and resulted in expected modulation depths of 45, 35 and 20% at 5, 10 and 20 MHz, respectively; the circuit would use 5 W RF power. The second solution consists of a signal generator, a broadband RF amplifier, a step transformer, an impedance matching network and the cell. Since the impedance of the crystal, being almost purely capacitive, varies with the modulation frequency, a multiple frequency impedance matching network would have to be designed in order to transform the load impedance into a constant of about 500 Ω. Networks at multiple frequencies are usually designed by combining more inductive and capacitive elements in a regular L-type network [12]. A 3:1 step-up transformer would convert that impedance into a regular 50Ω, thus matching the output impedance of a regular RF amplifier. The overall cost for such solution would be about $7000-8000. Usually RF amplifiers have to be connected to matched loads to avoid damage. There are, however, amplifiers that are built in such a way that they can be used with unmatched loads, and therefore would not require an impedance matching network. A quote for one of such amplifiers was obtained from *Electronics & Innovation, Ltd.* for a broadband (0.3-35 MHz) 300 W amplifier and 3:1 transformer, which would be $22000. A third solution was devised by Charles Moeller (GA) and consists of a variable inductor and a variable capacitor that would create a resonant circuit with the cell at various frequencies. The voltage in the circuit would be sampled and provided to a

field effect transistor, thus providing a feed-back loop that creates an oscillator at the frequency set by the oscillator. The input oscillating voltage would be amplified a first time by the operational amplifier, and a second time by the tank resonant circuit. Such solution would be obtained with $1000 in components and is sketched in fig.8.

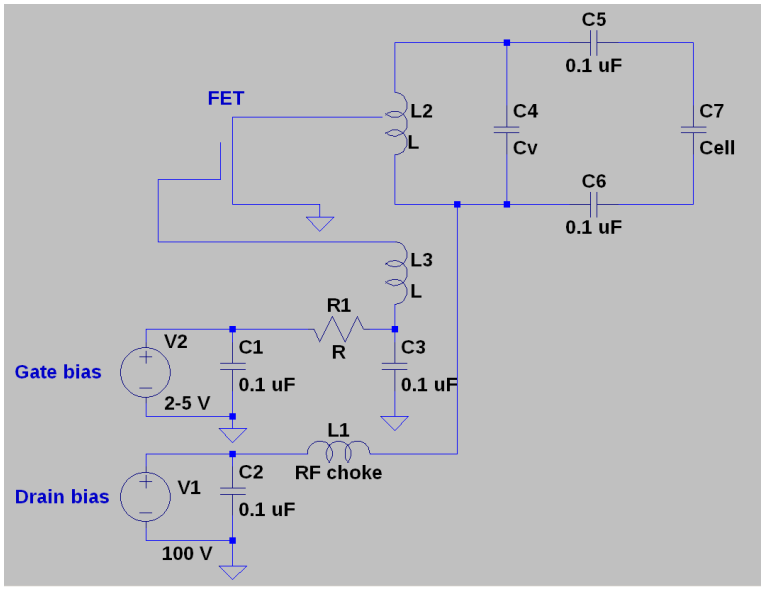

Figure 8: Sketch diagram of the third solution described in the text.

This solution was the one adopted in the actual fabrication of the driver; the variable capacitance and the transistor were procured, while the inductor was manufactured in house. A picture of the resulting circuit is shown in fig.9, where operation with 2 kV oscillating at 10 MHz frequency is visible on the probing oscilloscope.

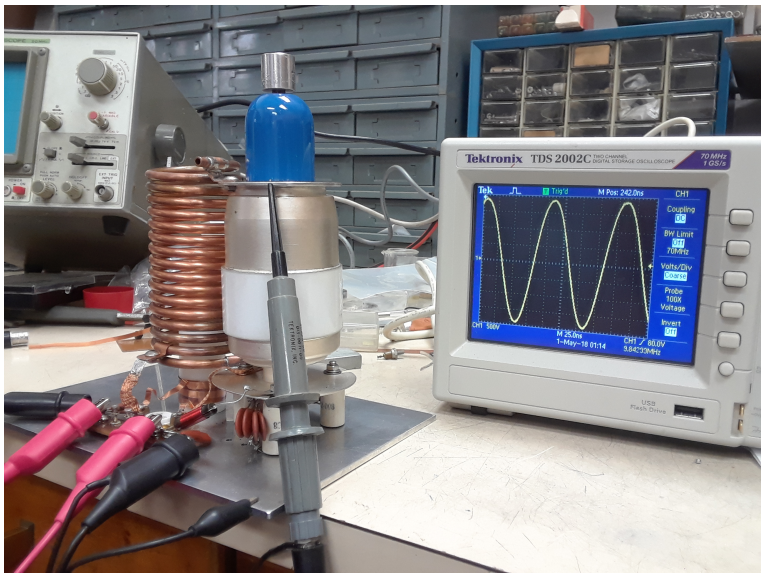

Figure 9: Picture of C.Moeller's resonant circuit, in which the two largest components are the variable inductor and capacitor. The resulting high voltage modulated at 10 MHz is visible on the oscilloscope.

References

[1] D.H. Goldstein, *Polarized Light, Third Edition*, CRC press

[2] Cécile Malgrange, Christian Ricolleau and Michel Schlenker, *Symmetry and Physical Properties of Crystals*, Springer.

[3] M. Bass *Handbook of Optics*, McGraw-Hill

[4] A. Yariv *Optical waves in crystals*, Wiley interscience 2003.

[5] S. Coda, *An Experimental Study of Turbulence by Phase Contrast Imaging on the DIII-D Tokamak*, MIT 1997

[6] W.L Wolfe and G.J Zissis, *The infrared handbook* Ann Arbor, Mich. : Environmental Research Institute of Michigan, 1985

[7] M. Porkolab at al., *Measurement of Helicons and Parametric Decay Waves in DIII–D with Phase Contrast Imaging* 2015 submitted to DoE for funding.

[8] Y. Tsay, B. Bendow and S. Mitra, *Phys. Rev B* **8** (1973) 2688

[9] J. Ptasinski, I.C. Khoo and Y. Fainman, *Materials* **7** (2014) 2229

[10] C. Cohen-Tannoudji, B. Diu and F. Laloe, *Quantum mechanics*, Wiley-VCH

[11] M.E. Courtney, *IEEE Trans. on Microwave Theory and Technique* **25** (1977) 697

[12] N. Nallam and S. Chatterjee, *IEEE trans. on circuits and systems* **60** (2013) 1635